THE JOURNAL OF BIOLOGICAL CHEMISTRY Vol. 278, No. 41, Issue of October 10, pp. 39747–39754, 2003
Printed in U.S.A.

Exploration of Ligands to the Q_i Site Semiquinone in the bc_1 Complex Using High-resolution EPR*

Received for publication, June 4, 2003, and in revised form, July 16, 2003
Published, JBC Papers in Press, July 21, 2003, DOI 10.1074/jbc.M305913200

Derrick R. J. Kolling‡§, Rimma I. Samoilova§¶‖, J. Todd Holland‡, Edward A. Berry, Sergei A. Dikanov‡‡, and Antony R. Crofts‡‖§§**

*From the Departments of ‖Biochemistry and ‡‡Veterinary Clinical Medicine and the ‡Center for Biophysics and Computational Biology, University of Illinois, Urbana, Illinois 61801, ¶Institute of Chemical Kinetics and Combustion, Russian Academy of Sciences, Novosibirsk 630090, Russia, and **Lawrence Berkeley National Laboratory, University of California, Berkeley, California 94720*

Pulsed EPR spectroscopy was used to explore the structural neighborhood of the semiquinone (SQ) stabilized at the Q_i site of the bc_1 complex of *Rhodobacter sphaeroides* (EC 1.10.2.2) and to demonstrate that the nitrogen atom of a histidine imidazole group donates an H-bond to the SQ. Crystallographic structures show two different configurations for the binding of ubiquinone at the Q_i site of mitochondrial bc_1 complexes in which histidine (His-201 in bovine sequence) is either a direct H-bond donor or separated by a bridging water. The paramagnetic properties of the SQ formed at the site provide an independent method for studying the liganding of this intermediate species. The antimycin-sensitive SQ formed at the Q_i site by either equilibrium redox titration, reduction of the oxidized complex by ascorbate, or addition of decylubihydroquinone to the oxidized complex in the presence of myxothiazol all showed similar properties. The electron spin echo envelope modulation spectra in the ^{14}N region were dominated by lines with frequencies at 1.7 and 3.1 MHz. Hyperfine sublevel correlation spectroscopy spectra showed that these were contributed by a single nitrogen. Further analysis showed that the ^{14}N nucleus was characterized by an isotropic hyperfine coupling of ~0.8 MHz and a quadrupole coupling constant of ~0.35 MHz. The nitrogen was identified as the N-ϵ or N-δ imidazole nitrogen of a histidine (it is likely to be His-217, or His-201 in bovine sequence). A distance of 2.5–3.1 Å for the O–N distance between the carbonyl of SQ and the nitrogen was estimated. The mechanistic significance is discussed in the context of a dynamic role for the movement of His-217 in proton transfer to the site.

The bc_1 complex family of enzymes plays a central role in all the main pathways of energy conversion, being directly responsible for ~30% of all the energy transduction of the biosphere (1–3). The complexes in *Rhodobacter* exemplify the simplest of these enzymes, with only three or four subunits, including the highly conserved catalytic core common to bacterial and mitochondrial complexes. It is generally accepted that the complex operates through a protonmotive Q cycle (2, 4, 5). Three catalytic subunits, cytochrome *b*, cytochrome c_1, and the Rieske iron-sulfur protein, house the mechanism. Two separate internal electron transfer chains connect three catalytic sites for external substrates. At one site, cytochrome c_1 is oxidized by cytochrome c_2. Two catalytic sites in cytochrome *b* are involved in the oxidation or reduction of ubiquinone. At the quinol oxidizing site, one electron from quinol is passed to the iron-sulfur protein, which transfers it to cytochrome c_1, whereas the semiquinone (SQ)[1] produced is oxidized by another chain consisting of the two b-hemes of cytochrome *b* in the bifurcated reaction. At the quinone-reducing site (Q_i site), electrons from the b-heme chain are used to generate quinol. The integration of the oxidation and reduction reactions with the release or uptake of protons in the aqueous phases allows the complex to pump protons across the membrane. Electron transfer between the two Q sites through the b-heme chain provides the main electrogenic contribution.

The Q_i site operates as a two-electron gate in which heme b_H reduces Q to SQ on one turnover of the quinol oxidizing site and SQ to QH_2 on the second turnover (6, 7). The SQ intermediate can also be generated as a thermodynamically stable species by redox (8, 9) or coulometric (10) titration, or by reversal of the second electron transfer (11, 12). However, details of the equilibrium and rate constants, the interaction between semiquinone and heme b_H, and the specific role of ligands in catalysis remain unresolved (8, 14–16). In each of these approaches, the yield of SQ, whether measured kinetically or thermodynamically, has always been substantially less than the stoichiometry of bc_1 complex (~0.4 under conditions giving maximal yield). Early work from de la Rosa and Palmer (10) suggested the explanation that this might reflect spin silencing from magnetic interaction with oxidized heme b_H. In this case, two populations of SQ might be expected, one with a fast and the other with a slow relaxation. The properties reported in the

* This work was supported by National Institutes of Health Grants GM 35438 (to A. R. C.) and GM 62954 (to S. A. D.), Fogarty Grant PHS 1 R03 TW01495 (to A. R. C. and R. I. S.), and NCRR/National Institutes of Health Grant S10-RR15878 for instrumentation. The costs of publication of this article were defrayed in part by the payment of page charges. This article must therefore be hereby marked "*advertisement*" in accordance with 18 U.S.C. Section 1734 solely to indicate this fact.

We dedicate this paper to the memory of Professor Arnold Hoff of the Biophysics Department at Leiden University, The Netherlands, who was an inspiration to all who worked in the field of advanced EPR and the areas of photosynthesis and biological electron transfer. Arnold was not only at the forefront of these fields but was also highly innovative in the development of new techniques and applications to research in this area. He will be sorely missed.

The atomic coordinates and structure factors (code 1pp9) have been deposited in the Protein Data Bank, Research Collaboratory for Structural Bioinformatics, Rutgers University, New Brunswick, NJ (http://www.rcsb.org/).

§ Both authors contributed equally to this work.

§§ To whom correspondence should be addressed: Dept. of Biochemistry, University of Illinois, 419 Roger Adams Laboratory, 600 South Mathews Ave., Urbana, IL 61801. Tel.: 217-333-2043; Fax: 217-244-6615; E-mail: a-crofts@life.uiuc.edu.

[1] The abbreviations used are: SQ, ubisemiquinone; bc_1 complex, ubihydroquinone:cytochrome *c* oxidoreductase; ENDOR, electron nuclear double resonance; ESEEM, electron spin echo envelope modulation; H-bond, hydrogen bond; HYSCORE, hyperfine sublevel correlation spectroscopy; Q or quinone, ubiquinone; QH_2 or quinol, ubihydroquinone; Q_i site, site of bc_1 complex at which quinone is reduced; CHES, (2-(cyclohexylamino)ethanesulfonic acid); MOPS, 4-morpholinepropanesulfonic acid; N-δ, imine nitrogen; N-ϵ, amine nitrogen.

literature are those of a slowly relaxing species, easily saturated at a temperature < 100 K.

The crystallographic structures (17–20) provide a molecular context in which a number of these unresolved mechanistic questions can be addressed more effectively. However, a better understanding of the binding of the different components of the Q/SQ/QH_2 system at the Q_i site requires additional structural information related to transient states. The two high-resolution structures show different configurations of the site; in the yeast complex (20), His-202 is rotated out of the site and contacts the quinone occupant through a bound water. In the bovine complex, His-201 is H-bonded directly to the quinone occupant.

The paramagnetic properties of the intermediate SQ species provide an opportunity to explore the local environment through high-resolution EPR techniques such as ENDOR (electron nuclear double resonance) and ESEEM (electron spin echo envelope modulation) (21). By using these techniques, answers to the following questions can be addressed directly by measurement of the interaction between the paramagnetic center and nuclear spins from atoms in the immediate protein and solvent environment. (i) What are the liganding atoms for the SQ? (ii) Are waters involved directly in ligation? (iii) Does the configuration of the site in the presence of SQ differ from either of the x-ray structures?

In previous work (22), the ubisemiquinone at the Q_i site was studied by ENDOR. Spectra showed a loss of intensity (most significantly at the frequencies ±2 MHz from the proton Zeeman frequency) after H/D exchange. These changes were assigned to one or more protons from hydrogen bonds, but the number of hydrogen bonds, their orientation, and which protein atoms were involved in these bonds were not resolved. The ENDOR spectra reported did not show the low frequency range (<10 MHz) where nitrogen peaks are usually located.

In this paper, we report a study of SQ intermediate formed at the Q_i site in the bc_1 complex from *Rhodobacter sphaeroides* (EC 1.10.2.2) by one-dimensional and two-dimensional ESEEM techniques and demonstrate that a nitrogen atom characteristic of a histidine imidazole group provides an H-bond to the SQ.

EXPERIMENTAL PROCEDURES

Preparation of Isolated bc_1 Complex—The bc_1 complex was isolated from chromatophores prepared from *R. sphaeroides* strain GBH6 and purified by following the protocols described by Kuras *et al.* (23) with minor modifications as follows: the concentration of chromatophores was adjusted to give an absorbance of $\Delta A_{562-577\ nm} = 1.2$, and solubilization was performed for 1 h. The bc_1 complex was used fresh (freezing requires cryoprotectants (Me_2SO or glycerol), which decrease the amplitude of the Q_i site semiquinone).

Generation of Semiquinone at the Q_i Site—Three protocols were used to generate semiquinone at the site. 1) The isolated bc_1 complex at 50–200 μM was suspended in a medium containing 100 mM KCl, 50 mM MOPS, 5 mM $MgSO_4$, 0.01% *n*-dodecyl-β-D-maltoside (Sigma), 15 μg/ml phosphatidylcholine (Avanti Polar-Lipids, Inc., Alabaster, AL) at pH 7.8, 18–20 °C and reduced by the addition of sodium ascorbate, pH 7.0, to give a final concentration of 1 mM. Samples were incubated for 5 min and then stored under liquid N_2 until used for spectroscopy. 2) The bc_1 complex at 50–200 μM was suspended in a medium containing 100 mM KCl, 50 mM CHES, 5 mM $MgSO_4$, 0.01% *n*-dodecyl-β-D-maltoside, 15 μg/ml phosphatidylcholine at pH 9.0, 18–20 °C in a redox titration cell which was kept anaerobic by argon gas. Redox mediators present were 40 μM 1,2-naphthoquinone and 40 μM 1,4-naphthoquinone. The redox potential was adjusted by the addition of small aliquots of dithionite or ferricyanide, and samples were taken under anaerobic conditions at the desired E_h values using a syringe, placed in an EPR tube previously flushed with argon, frozen, and stored in liquid N_2 until use. 3) The bc_1 complex at 50–200 μM was suspended in a medium containing 100 mM KCl, 50 mM CHES, 5 mM $MgSO_4$, 0.01% *n*-dodecyl-β-D-maltoside, 15 μg/ml phosphatidylcholine, and excess myxothiazol at pH 9.0 and reduced by the addition of decylubihydroquinone in 2-fold molar excess over the bc_1 complex monomer concentration. Samples were immediately stored under liquid N_2 until used for spectroscopy.

In all cases, the semiquinone species observed was completely eliminated by the addition of antimycin at 2-fold molar excess over the monomer concentration.

EPR Measurements—The EPR and ESEEM experiments were carried out using an ELEXSYS E580 X-band spectrometer (Bruker) with an Oxford CF 935 cryostat. Several types of ESEEM experiments with different pulse sequences were employed, with appropriate phase-cycling schemes to eliminate unwanted features from experimental echo envelopes. Among them were two pulse sequences and one- and two-dimensional three- and four-pulse sequences. In the two-pulse experiment ($\pi/2 - \tau - \pi - \tau -$ echo), the intensity of the echo signal at fixed interval, τ, between two microwave pulses with spin vector rotation angles $\pi/2$ and π is measured as a function of the magnetic field. In the one-dimensional three-pulse experiment ($\pi/2 - \tau - \pi/2 - T - \pi/2 - \tau -$ echo), the intensity of the stimulated echo signal after the third pulse is recorded as a function of time, T, at constant time, τ. The set of three-pulse envelopes recorded at different τ values forms a two-dimensional three-pulse data set. In the two-dimensional four-pulse experiment ($\pi/2 - \tau - \pi/2 - t_1 - \pi - t_2 - \pi/2 - \tau -$ echo, also called HYSCORE), the intensity of the stimulated echo after the fourth pulse was measured with t_2 and t_1 varied and τ constant. Spectral processing of three- and four-pulse ESEEM patterns was performed using WIN-EPR software (Bruker).

Crystallography—Conditions for crystallography are described in detail in file 1pp9 and supplementary materials deposited with the Protein Data Bank and will be published elsewhere.

RESULTS AND DISCUSSION

Structures of the bc_1 complex from several groups have been reported in which an endogenous ubiquinone occupies the Q_i site. In the structures of the complex from chicken mitochondria from Berry and co-workers (17) (Protein Data Bank accession numbers 1bcc and 2bcc; Refs. 17 and 24), the quinone was shown with three groups from the cytochrome *b* peptide chain within H-bonding distance, His-202 and Asp-229 side chains forming ligands to the carbonyl oxygens, and Ser-206 side chains forming ligands to a methoxy oxygen atom. A structure at higher resolution from Hunte *et al.* (Protein Data Bank accession number 1evz; Ref. 20) showed a different configuration in which the equivalent residues were involved but with His-202 rotated away from the quinone occupant and with water bridging between the quinone (>C=O) and the histidine. In Fig. 1, we compare this latter structure to the Q_i site configuration in a new high-resolution structure (Protein Data Bank accession number 1pp9 at 2.1 Å) of the bovine mitochondrial complex. In this configuration, the arrangement of the ligands is similar to that from the earlier chicken complex but clearly different from the yeast structure. The three potential H-bonds are His-201 N-ϵH to >C=O (2.52 Å), Asp-228 –OH to >C=O (2.74 Å), and Ser-205 –OH to the H_2O (2.62 Å) and to the –O-CH_3 oxygen atom (4.06 Å).

The SQ at the Q_i site has been studied most completely in the context of redox titrations of the signal detected by continuous wave-X-band EPR (8, 9, 14, 15). From the pH dependence, it has been concluded that the anion is the stable species, and parameters have been proposed that describe the stability in terms of the disproportionation reaction, midpoint redox potential (E_m) values for the two half-cell reactions, and pK values for the dissociable forms. The SQ can also be formed by reversal of the forward reaction on addition of QH_2 to the isolated complex in a myxothiazol-insensitive, antimycin-sensitive reaction (11, 12).

The continuous wave EPR spectrum of ascorbate-reduced samples of the bc_1 complex in frozen solution shows an anisotropic powder line shape with a rhombic g-tensor $g_1 = 2.01$, $g_2 = 1.91$, $g_3 = 1.80$ from the reduced Rieske [2Fe-2S] cluster. In many published spectra, and also in the isolated complex, an additional overlapping spectrum with a narrow line (width = 0.8 mT) at $g \sim 2$ is also seen. We observed that this narrow line disappeared with the addition of antimycin, indicating a phe-

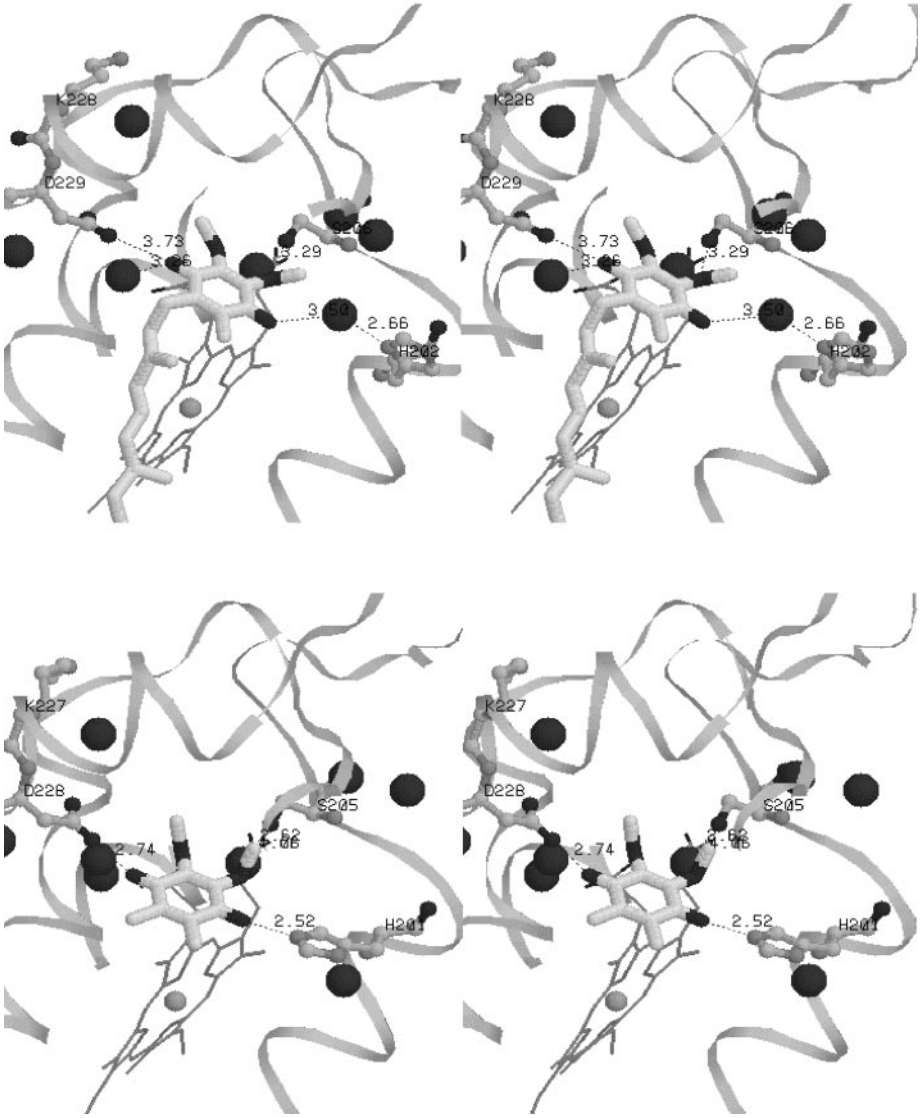

FIG. 1. **The ligands to the quinone occupant of the Q_i site of mitochondrial bc_1 complexes.** The protein backbone around the Q_i site is shown for the bc_1 complex from (*top*) yeast mitochondria (Protein Data Bank accession number 1ezv; Ref. 20) and from (*bottom*) bovine mitochondria (Protein Data Bank accession number 1pp9). Residues acting as direct or indirect ligands are shown as *ball-and-stick models* in *gray*, with nitrogen atoms in *darker gray* and oxygen atoms in *black*. The quinone occupant is shown as a *tube model*, with carbon atoms in *light gray* and oxygen atoms in *black*. The heme b_H is shown as a *stick model*, with carbon atoms in *gray* and the iron atom as a *gray sphere*. Water oxygen atoms are shown as *black space-filling spheres*. The protein backbone is shown as a *gray ribbon*. The two models were manipulated to show a similar orientation of the heme. Images are presented in stereo views for crossed-eye viewing.

nomenological association with the Q_i site. We have compared the properties of the species generated on the addition of ascorbate with those of the semiquinone formed by equilibrium redox titration at high pH and with the semiquinone generated on reversal of the normal forward reaction on addition of decylubihydroquinone to the oxidized complex in the presence of myxothiazol. The EPR relaxation times at 90 K and the line widths of the semiquinone generated under these three conditions were essentially the same. In view of the different procedures used, this result is significant, because previous studies had indicated that a substantial fraction of the semiquinone signal generated on one-electron reduction through a mediator was invisible, perhaps because of spin coupling to a neighboring oxidized b-heme (10). The similarity of the properties of the semiquinone generated by these three different procedures suggested that if such a spin coupling occurs, it has a relaxation time faster than the microsecond scale and does not affect the properties of the signal explored here.

The similarity of the EPR spectrum of the signal from SQ generated by three different procedures, the good correlation with properties previously reported, and its sensitivity to antimycin allow us to assign the narrow line to the SQ intermediate at the Q_i site of the bc_1 complex. To explore the local environment of the semiquinone, we used pulsed EPR to determine the nature of neighboring nuclear spins. In the experiments shown in Figs. 2 and 3, the ascorbate-reduced sample was used, and similar spectra were obtained with all three samples.

Although the line from SQ overlaps with the signal of the Rieske cluster in continuous wave EPR spectrum, the characteristics of a pure SQ signal without any contamination from the cluster could be studied using pulsed EPR by exploiting the different temperature dependence of the relaxation times for the echo signals from the SQ and Rieske cluster.

Fig. 2*a* shows field-sweep two-pulse ESE spectrum of the bc_1 complex recorded at 90 and 30 K. The single line of SQ is the only one present in the 90 K spectrum; line shape characteris-

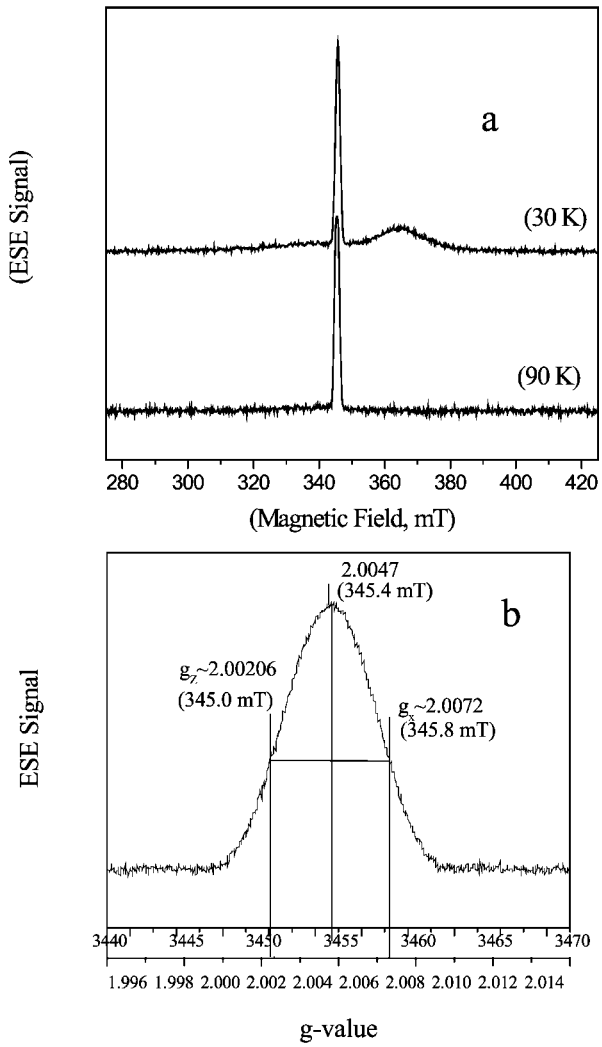

FIG. 2. **Two-pulse field sweep ESE spectra of the semiquinone at the Q_i site.** *a*, the spectrum recorded at 30 K (*top*) and at 90 K. *b*, characteristics of the SQ line at 90 K. Microwave frequency was 9.70 GHz, τ = 120 ns.

tics are shown at higher sensitivity in Fig. 2*b*. The relaxation time of the two-pulse echo of the Rieske cluster is too short (less then several hundred ns) at 90 K for its contribution to be detected in the spectrum; the echo signal from the Rieske cluster can only be observed at $T < 30$ K.

The T_1 relaxation measured at the peak height showed at all temperatures a small rapid component. This was of increasing significance as the temperature was lowered and likely includes a contribution from the Rieske cluster. This rapid relaxing component was not explored in greater detail in this study. However, we note that the selection procedure used here would also eliminate any rapidly relaxing semiquinone signal.

Fig. 3*a* shows stacked plots of three-pulse ESEEM spectra at frequencies <10 MHz, which are appropriate for detection of ^{14}N nuclei, recorded as a function of time, τ, between the first and second pulses. These spectra contain two lines at 1.7 and 3.1 MHz, which indicate the presence of [^{14}N]nitrogen in the immediate neighborhood of the SQ that interact with its unpaired spin.

Additional information about the relations between the different nitrogen frequencies observed was obtained from two-dimensional HYSCORE spectra. The non-diagonal cross-peaks in HYSCORE spectra correlate nuclear frequencies from the different electron spin manifolds belonging to the same nucleus. Fig. 3*b* shows a typical HYSCORE spectrum which contains only two off-diagonal cross-peaks in the (++) quadrant, correlating frequencies 1.7 and 3.1 MHz. The contour line shape of these cross-peaks is circular, indicating the absence of any significant anisotropy of the corresponding transitions which would otherwise produce ellipsoid contour line shapes. There are no other well pronounced correlations, probably because of the extended anisotropic character of other transitions in both electron spin manifolds.

^{14}N can produce up to six lines in ESEEM spectrum, three from each of two electron spin manifolds with $m_S = +½$ or $-½$. Because of their different orientation dependence, not all transitions contribute equally to the spectra when measurements are made using amorphous samples (powder-type samples, as in the case of the frozen suspensions of the bc_1 complex used in these experiments). The type of powder ESEEM spectrum expected from ^{14}N with isotropic hyperfine coupling A is governed by the ratio between the effective nuclear frequency in each manifold, $\nu_{ef\pm}$, given by $\nu_{ef\pm} = |\nu_I \pm A/2|$, and the quadrupole coupling constant, K, given by $K = e^2qQ/4h$ (25).

If $\nu_{ef\pm}/K < 1$, then the three nuclear frequencies in a corresponding manifold will be close to three pure nuclear quadrupole resonance frequencies of ^{14}N, which would produce three narrow peaks at

$$\nu_+ = K(3 + \eta) \qquad \nu_- = K(3 - \eta) \qquad \nu_o = 2K\eta \qquad \text{(Eq. 1)}$$

with the property $\nu_+ = \nu_- + \nu_o$, where the term η is an asymmetry parameter. However, such lines are not present in the ESEEM spectra reported here, so we can exclude this case from consideration.

If $\nu_{ef\pm}/K > 1$, only a single narrow line from each corresponding manifold is expected, produced by a transition at the maximal frequency, which is actually a double-quantum transition between two outer states with $m_I = -1$ and 1. The frequency of this transition is described by the formula

$$\nu_{dq\pm} = 2[\nu^2_{ef\pm} + \kappa]^{1/2} \qquad \text{(Eq. 2)}$$

where $\kappa = K^2(3 + \eta^2)$. Two other single-quantum transitions, involving the central level with $m_I = 0$, have a significant orientation dependence from quadrupole interaction and do not produce informative narrow lines.

The observation of only two narrow peaks at 1.7 and 3.1 MHz in three-pulse ESEEM spectra belonging to opposite manifolds indicates a ^{14}N with both ratios $\nu_{ef+}/K > 1$ and $\nu_{ef-}/K > 1$. These peaks could, therefore, be assigned to the double-quantum transitions ν_{dq+} = 3.1 MHz and ν_{dq-} = 1.7 MHz.

Formal application of Equation 2 to the observed frequencies of 1.7 and 3.1 MHz with ν_I = 1.06 MHz provides values of A = 0.8 MHz and κ = 0.43 MHz^2. Assuming a variation for η between 0 and 1 ($0 \le \eta \le 1$), the value for κ leads to $K = 0.35 \pm 0.3$ MHz. For these values of A and K, the $\nu_{ef\pm}/K$ values are 4.2 and 1.9, respectively, providing support for the assignment of both frequencies to a single ^{14}N and for the analytic procedure used. Simulation of the ESEEM spectra also supports this assignment and reproduces the appearance of 1.7 and 3.1 MHz peaks.

Thus, analysis of the ESEEM spectra shows interaction of the SQ spin with a single nitrogen characterized by an isotropic hyperfine coupling, A, of ~0.8 MHz and a quadrupole coupling constant, K, of ~0.35 MHz. This isotropic hyperfine coupling suggests the existence of an atomic bridge for the transfer of spin density from the SQ on this protein nitrogen. The only likely mechanism for such a transfer is a hydrogen bond between one of the SQ oxygens and the protein nitrogen identified.

The value of the quadrupole coupling constant K determined above allows us to reach a firm conclusion about the type of

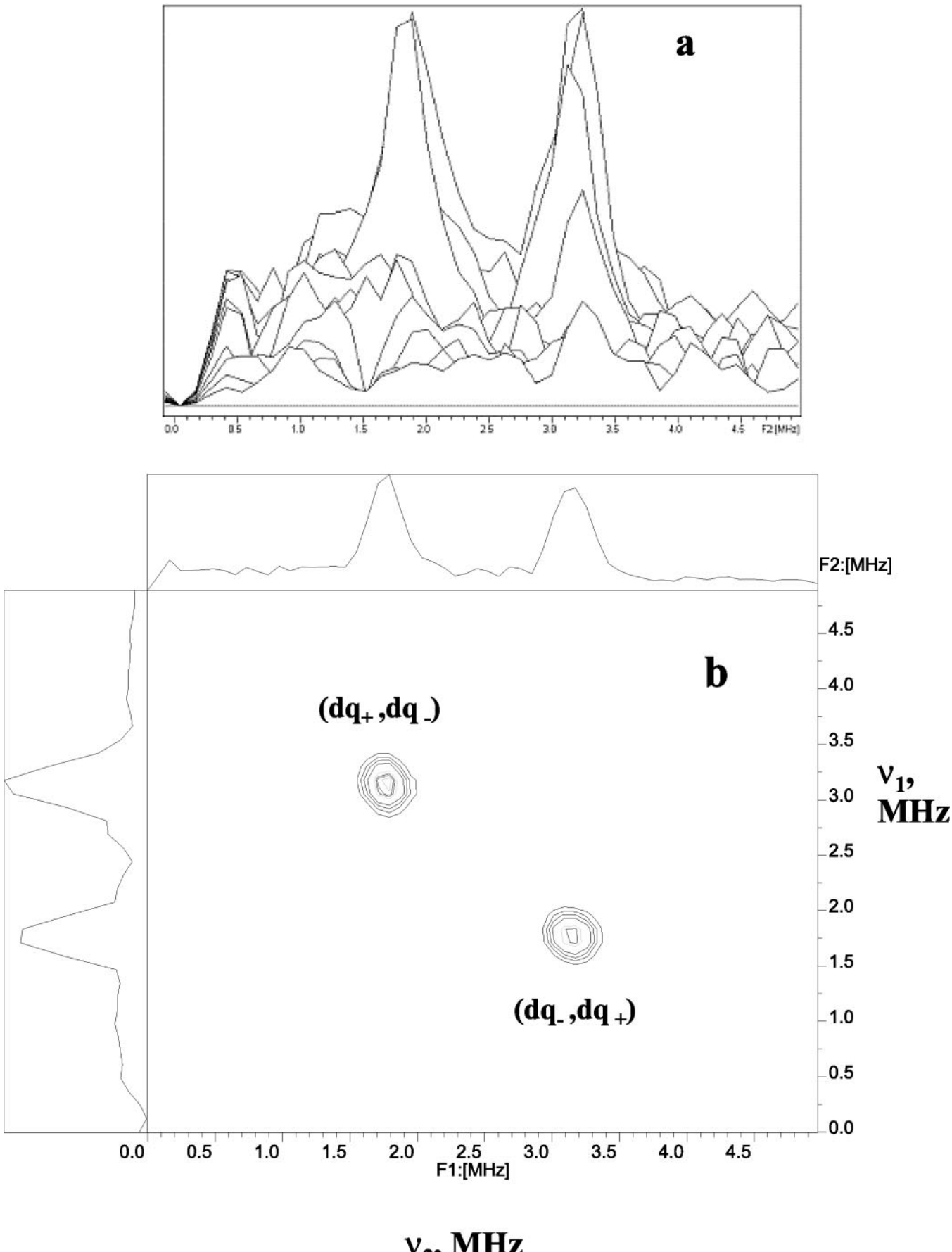

FIG. 3. **ESEEM spectra of the SQ at the Q_i site.** *a*, representative stacked plot of three-pulse ESEEM. The spectra show the modulus of Fourier transform along time T axis. The initial τ is 88 ns in the farthest trace and was increased by 16 ns in successive traces. Microwave frequency was 9.70 GHz and magnetic field was 354.2 mT. *b*, HYSCORE spectrum measured with τ = 200 ns and other parameters as above.

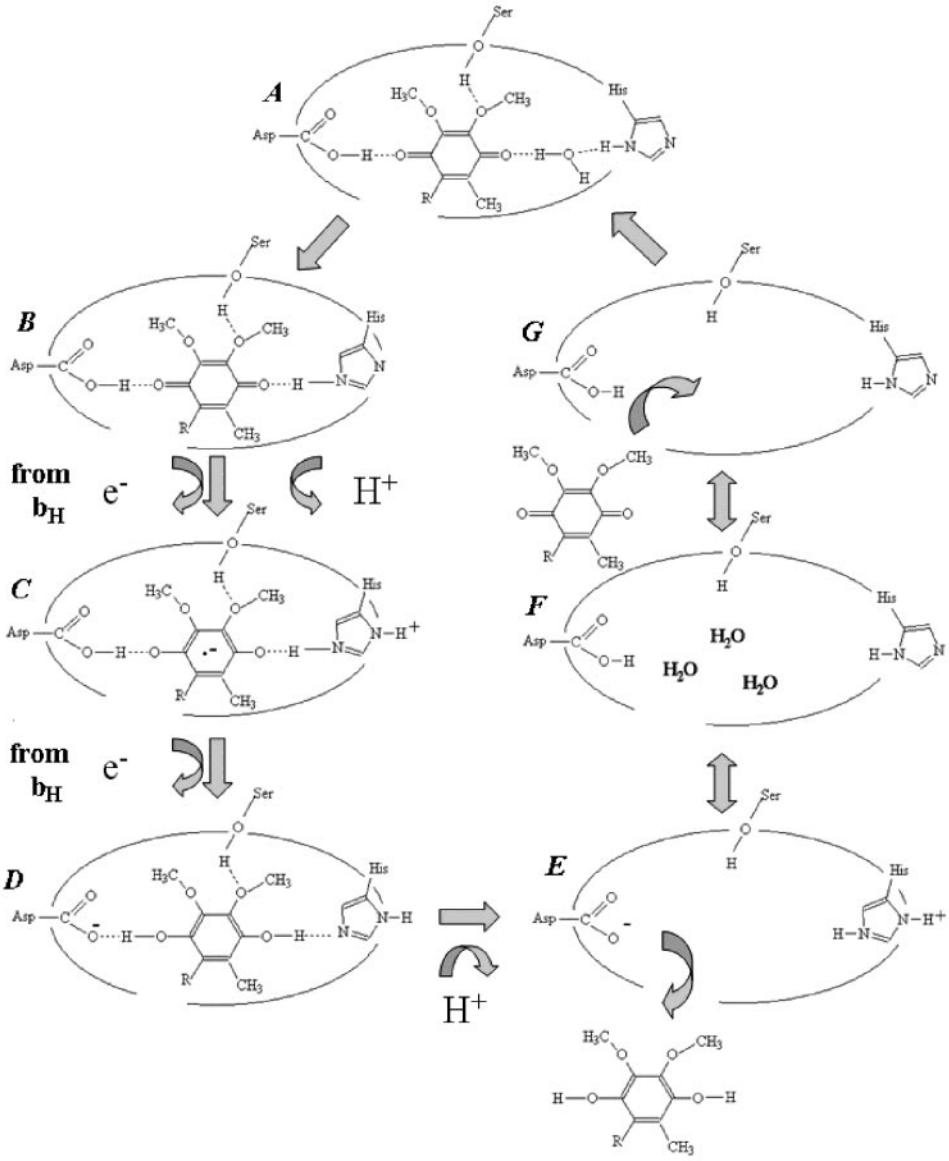

FIG. 4. **Scheme showing proposed involvement of liganding groups in the function of the Q_i site.** The different occupants of the site are shown for different states of the cycle of reactions at the Q_i site, which is shown in the direction of forward electron flow. State *A* might represent the structure of Hunte *et al*. (20), state *B* represents the structure of Berry and co-workers (24), and state *C* represents the structure determined here by ESEEM. The second electron transfer is reversible, so that formation of the semiquinone from QH_2 upon addition to the oxidized complex would be represented by reversal of transitions leading to the formation of state *A* from *C*. No attempt has been made to show the many different states of protonation of the residues involved, and the particular points of entry of H^+ in the scheme should, therefore, be regarded as flexible and would change with pH.

nitrogen involved in the interaction with SQ and to correlate it with crystallographic structures of the mitochondrial bc_1 complexes. Because the experiments reported here were performed with the bc_1 complex from *R. sphaeroides*, we must first consider how the Q_i site in this complex aligns with those from the mitochondrial complexes. Fortunately, sequence alignments show that the spans containing the liganding residues are highly conserved, and a structure of the *Rhodobacter capsulatus* bc_1 complex at 3.5-Å resolution[2] shows that the tertiary structure for these spans is also conserved. From the alignments and the structure, the residues likely acting as ligands are His-217 (His-202), Asn-221 (Ser-206), and Asp-252 (Asp-229) (residues in parentheses are yeast or chicken equivalents; for the bovine sequence, subtract 1). Strong support for an important role in catalysis has come from mutagenesis of each of these residues in both *Rhodobacter* species (16, 26, 27). From alignment with the mitochondrial structures, there are no other side-chain or backbone nitrogen atoms that could be expected to interact with the semiquinone. Therefore, we can confine our discussion to the two residues with potential nitrogen ligands in the immediate neighborhood of quinone in the Q_i site; His-217 with the two nitrogen atoms of the imidazole ring, and Asp-221 with the $-NH_2$ group of the amide side chain. Values for *K* from amino acid side chains have been studied extensively. For ^{14}N of the side-chain $-NH_2$ group in L-asparagine, the value for *K* measured by nuclear quadrupole resonance is 0.63 MHz (28). The nuclear quadrupole resonance method also provides a value for the asymmetry parameter, $\eta = 0.39$, which allows us to calculate a value for κ of 1.25 MHz[2]. Values for both *K* and κ for this nitrogen are far removed from the *K* and κ values for the ^{14}N estimated from the ESEEM spectra here.

The quadrupole parameters reported for imine (N-δ) and amine (N-ϵ) nitrogens in non-coordinated imidazole and histi-

[2] E. Berry and F. Daldal, personal communication.

dine are equal to $K = 0.81–0.84$ MHz ($\eta = 0.13$), $\kappa = 1.98–2.12$ MHz^2, and $K = 0.35$ MHz, ($\eta = 0.915–0.995$) and $\kappa = 0.47–0.49$ MHz^2, respectively (29–31). However, when both imidazole nitrogens are protonated, as in L-histidine monochloride monohydrate, then the quadrupole parameters become $K = 0.32$ MHz ($\eta = 0.946–0.974$) and $\kappa = 0.40$ MHz^2 for N-δ, and $K = 0.366$ MHz ($\eta = 0.268–0.3$) and $\kappa = 0.41$ MHz^2 for N-ε (31, 32). The similar values for κ (0.40–0.41) for both nitrogens is only slightly less than the value 0.43 MHz^2 derived from the ESEEM spectra reported here.

The H–O distance in hydrogen bonds for N-ε-H–O and Nδ-H–O in L-histidine hydrochloride are both 1.94 Å. This value is in good agreement with an estimate of the distance of exchangeable protons in hydrogen bonds (1.5–2.0 Å) around the SQ in the Q_i site of the bc_1 complex obtained from a proton ENDOR study by Salerno *et al.* (22). Because typical lengths for N-H-bonds for both nitrogens in histidine molecules are within 1.0–1.1 Å (33), one can estimate a value for the N–O distance in L-histidine hydrochloride at ~2.5–3.1 Å, depending on the –N–H–O angle. From the almost equal quadrupole parameters κ of the nitrogen interacting with SQ in the Q_i site compared with the nitrogens in L-histidine hydrochloride, we can conclude with some confidence that the N–O distance between the carbonyl oxygen of the SQ and an imidazole nitrogen of His-217 has a value between 2.5 and 3.1 Å. In the 2.1-Å resolution structure of the bovine mitochondrial complex, a similar value (2.52 Å) for the hydrogen bond length for interaction of His-201 with Q is found. Therefore, the bond lengths are similar for the EPR and crystallographic structures, although the bonds are probably to different quinone species.

The characteristics of the nitrogen involved in magnetic interaction with the SQ are also consistent with the previous studies of semiquinones that are liganded by histidines in photosynthetic reaction centers. The most recent ESEEM study of the semiquinone radical of Q_A^- in Photosystem II membranes at various pH values has reported the presence of two protein nitrogens magnetically coupled to the Q_A^- spin (34). One of them with $K = 0.82$ MHz and $A \sim 2.1$ MHz is assigned to an amide nitrogen from the protein backbone, whereas the second one with $K = 0.35$ MHz and $A \sim 1.7$ MHz is attributed to the imino nitrogen, N-δ, of an imidazole. The contributions of these nitrogens to the ESEEM spectra were pH-sensitive, in line with their involvement in hydrogen bonding with the SQ. Earlier, the formation of hydrogen bonds with N-δ histidine nitrogen ($K = 0.38$ MHz and $A = 1.1$ MHz) and with a peptide nitrogen ($K = 0.76$ MHz and $A = 1.8$ MHz) were reported for reduced primary acceptor quinone Q_A^- in reaction centers of *R. sphaeroides* (13). The quadrupole characteristics determined here for SQ in the Q_i site of the bc_1 complex almost exactly match the values assigned to an imidazole nitrogen of histidine in both reaction centers, thus providing additional support for our assignment and for the involvement of this nitrogen in hydrogen bonding to the semiquinone at the Q_i site.

On other hand, we did not find any evidence for the transfer of measurable unpaired spin density on the nitrogen of the $–NH_2$ of the Asn-221. This allows us to exclude hydrogen bond formation between this nitrogen and the >C=O group in the pH range of our experiments. Furthermore, no participation of peptide nitrogens in hydrogen bonds was detected. Therefore, the possibility of other hydrogen bonds with SQ remains an open question. However, it seems likely that a hydrogen bond formed with the methoxy oxygen would hold much less unpaired spin density than the carbonyl oxygen interacting with histidine nitrogen and would not generate a prominent feature in the ^{14}N spectra. The presence of this additional H-bonded nitrogen atom could be better tested by experiments with ^{15}N-labeled bc_1 complex, where the dipolar coupling would allow exploration at the expected distance. This isotopic substitution will also allow us to determine the anisotropic part of the hyperfine interaction for histidine nitrogen. Experiments to this end are in progress. We will also report separately on interactions with local protons and the changes on substitution of ^2H_2O, or after the addition of deuterated ubihydroquinone, separately.

We can conclude that the semiquinone generated at the Q_i site of the bc_1 complex from *R. sphaeroides*, either directly through reduction of heme b_H by ubiquinol or through equilibrium redox titration, is liganded by an H-bond from an imidazole nitrogen of histidine. It seems highly likely that this is His-217, equivalent to His-201 seen as a ligand to the quinone occupant in the bovine mitochondrial complex. This correlation also strongly suggests that the bovine structure shows a physiologically relevant configuration. The different configuration seen in the yeast complex raises the question of a dynamic role for this histidine (Fig. 4). We note that the crystallization conditions for the yeast structure included a pH ≈ 8.5, compared with the slightly acidic pH used for the crystallography of the bovine complex of Fig. 1. Formation of an H-bond with the >C=O of quinone would require a protonated nitrogen, shown as the N-ε in Fig. 1 (*bottom*), which is consistent with assignment of the N-ε as the group with a higher p*K*. However, both protonated and singly deprotonated forms are tautomeric, so interaction energies will be felt across the ring. Formation of the SQ from the QH_2 would be expected to release at least one proton because of the low p*K* of the QH_2^+ state. The redox titration data suggest that the SQ is anionic, so formation of the semiquinone from QH_2 might be expected to involve a second proton. Therefore, it seems possible that the groups forming H-bonds to the two oxygen atoms of the SQ are both hydrogen donors. In exploring different conditions for formation of the SQ in this study, the pH was varied from 7.5 to 9.0, without any obvious effect in the ^{14}N ESEEM spectra. We can further conclude that the nature of the nitrogen ligand did not change over this range. If the SQ is anionic, it would likely raise the p*K* of the histidine ligand so as to favor protonation. For the quinone, the strength of the H-bond might be expected to vary with protonation state, and the different crystallographic structures, therefore, might simply reflect the different ligand strengths for states populated at the different pH values for crystallization. The structures can be interpreted as showing a role for the histidine in the transfer of at least one proton into or out of the chemistry of the site. In the normal forward direction, the histidine may or may not be protonated on binding the quinone, depending on local pH. At physiological pH of the mitochondrial matrix, it would likely be deprotonated but would become protonated on formation of the SQ. Upon transfer of a second electron, the proton would be formally transferred to the quinol, leaving the histidine deprotonated on release after formation of the quinol. Rotation of the histidine away from its liganding configuration combined with the exit of the QH_2 would open up the site for population with additional water molecules. This would allow protonation of the aspartate ligand that presumably serves a similar H^+ donation function for the other >C=O group.

REFERENCES

1. Nitschke, W., Muehlenhoff, U., and Liebl, U. (1997) in *Photosynthesis: a Comprehensive Treatise* (Raghavendra, A., ed) pp. 285–304, Cambridge University Press, Cambridge, U K
2. Berry, E., Guergova-Kuras, M., Huang, L.-S., and Crofts, A. R. (2000) *Annu. Rev. Biochem.* **69,** 1007–1077
3. Degli Esposti, M., De Vries, S., Crimi, M., Ghelli, A., Patarnello, T., and Meyer, A. (1993) *Biochim. Biophys. Acta* **1143,** 243–271
4. Mitchell, P. (1976) *J. Theor. Biol.* **62,** 327–367
5. Crofts, A. R. (1985) *The Enzymes of Biological Membranes* (Martonosi, A. N., ed) Vol. 4, pp. 347–382, Plenum Publishing Corp., New York

6. Crofts, A. R., and Wraight, C. A. (1983) *Biochim. Biophys. Acta* **726,** 149–186
7. Crofts, A. R., Meinhardt, S. W., Jones, K. R., and Snozzi, M. (1983) *Biochim. Biophys. Acta* **723,** 202–218
8. Robertson, D. E., Prince, R. C., Bowyer, J. R., Matsuura, K., Dutton, P. L., and Ohnishi, T. (1984) *J. Biol. Chem.* **259,** 1758–1763
9. De Vries, S., Berden, J. A., and Slater, E. C. (1982) *Function of Quinones in Energy Conserving Systems* (Trumpower, B. L., ed) pp. 235–246, Academic Press, New York
10. de la Rosa, F. F., and Palmer, G. (1983) *FEBS Lett.* **163,** 140–143
11. De Vries, S., Albracht, S. P. J., Berden, J. A., Marres, C. A. M., and Slater, E. C. (1983) *Biochim. Biophys. Acta* **723,** 91–103
12. Kauten, R., Tsai, A.-L., and Palmer, G. (1985) *J. Biol. Chem.* **262,** 8658–8667
13. Spoyalov, A. P., Hulsebosch, R. J., Shochar, S., Gast, P., and Hoff, A. J. (1996) *Chem. Phys. Lett.* **263,** 715–720
14. Salerno, J. C., Xu, Y., Osgood, P., Kim, C. H., and King, T. E. (1989) *J. Biol. Chem.* **264,** 15398–15403
15. Rich, P. R., Jeal, A. E., Madgwick, S. A., and Moody, A. J. (1990) *Biochim. Biophys. Acta* **1018,** 29–40
16. Crofts, A. R., Barquera, B., Bechmann, G., Guergova, M., Salcedo-Hernandez, R., Hacker, B., Hong, S., and Gennis, R. B. (1995) *Photosynthesis: From Light to Biosphere* (Mathis, P., ed) Vol. II, pp. 493–500, Kluwer, Dordrecht, The Netherlands
17. Zhang, Z., Huang, L.-S., Shulmeister, V. M., Chi, Y.-I., Kim, K.-K., Hung, L.-W., Crofts, A. R., Berry, E. A., and Kim, S-H. (1998) *Nature* **392,** 677–684
18. Xia, D., Yu, C.-A., Kim, H., Xia, J.-Z., Kachurin, A. M., Zhang, L., Yu, L., and Deisenhofer, J. (1997) *Science* **277,** 60–66
19. Iwata, S., Lee, J. W., Okada, K., Lee, J. K., Iwata, M., Rasmussen, B., Link, T. A., Ramaswamy, S., and Jap, B. K. (1998) *Science* **281,** 64–71
20. Hunte, C., Koepke, J., Lange, C., Rossmanith, T., and Michel, H. (2000) *Structure Fold Des.* **8,** 669–684
21. Hoff, A. J. (ed) (1989) *Advanced EPR Applications in Biochemistry and Biology*, Elsevier, Amsterdam, The Netherlands
22. Salerno, J. C., Osgood, M., Liu, Y., Taylor, H., and Scholes, C. P. (1990) *Biochemistry* **29,** 6987–6993
23. Kuras, R., Guergova-Kuras, M., and Crofts, A. R. (1998) *Biochemistry* **37,** 16280–16288
24. Crofts, A. R., Guergova-Kuras, M., Huang, L.-S., Kuras, R., Zhang, Z., and Berry, E. A. (1999) *Biochemistry* **38,** 15791–15806
25. Dikanov, S. A., Tsvetkov, Yu. D., Bowman, M. K., and Astashkin, A. V. (1982) *Chem. Phys. Lett.* **90,** 149–153
26. Hacker, B., Barquera, B., Crofts, A. R., and Gennis, R. B. (1993) *Biochemistry* **32,** 4403–4410
27. Gray, K. A., Dutton, P. L., and Daldal, F. (1994) *Biochemistry* **33,** 723–733
28. Hunt, M. J., and Mackay, A. L. (1974) *J. Magn. Reson.* **15,** 402–414
29. Edmonds, D. T., and Summers, C. P. (1973) *J. Magn. Reson.* **12,** 134–142
30. Hunt, M. J., Mackay, A. L., and Edmonds, D. T. (1975) *Chem. Phys. Lett.* **34,** 473–475
31. Hunt, M. J., and Mackay, A. L. (1976) *J. Magn. Reson.* **22,** 295–301
32. McDowell, C. A., Naito, A., Sastry, D. L., and Takegoshi, K. (1986) *J. Magn. Reson.* **69,** 283–292
33. Palmer, M. H. (1987) *Chem. Phys.* **1150,** 207–218
34. Deligiannakis, Y., Hanley, J., and Rutherford, A. W. (1999) *J. Am. Chem. Soc.* **121,** 7653–7664